Science of the Total Environment 615 (2018) 540–548

Contents lists available at ScienceDirect

Science of the Total Environment

journal homepage: www.elsevier.com/locate/scitotenv

The location- and scale- specific correlation between temperature and soil carbon sequestration across the globe

Jingyi Huang [a,b], Budiman Minasny [a,*], Alex B. McBratney [a], José Padarian [a], John Triantafilis [b]

[a] Sydney Institute of Agriculture & School of Life and Environmental Sciences, The University of Sydney, Eveleigh, NSW 2015, Australia
[b] School of Biological, Earth and Environmental Sciences, UNSW Sydney, NSW 2052, Australia

HIGHLIGHTS

- Negative correlation between SOC & temperature between 52°N and 40°S and vice versa
- SOC in low-temperature areas might increase under global warming and vice versa.
- Location- & scale- specific temperature effects important for soil carbon modeling

GRAPHICAL ABSTRACT

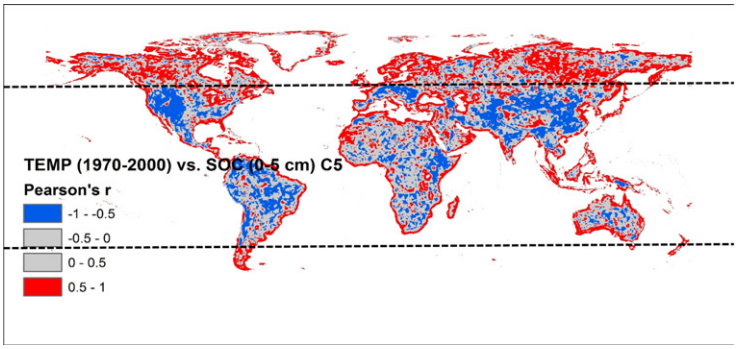

ARTICLE INFO

Article history:
Received 27 July 2017
Received in revised form 11 September 2017
Accepted 14 September 2017
Available online 6 October 2017

Editor: Ouyang Wei

Keywords:
Soil variability
Soil forming factor
Climate change
Carbon sink
Carbon pool

ABSTRACT

Much research has been conducted to understand the spatial distribution of soil carbon stock and its temporal dynamics. However, an agreement has not been reached on whether increasing global temperature has a positive or negative feedback on soil carbon stocks. By analysing global maps of soil organic carbon (SOC) using a spherical wavelet analysis, it was found that the correlation between SOC and soil temperature at the regional scale was negative between 52° N and 40° S parallels and positive beyond this region. This was consistent with a few previous studies and it was assumed that the effect was most likely due to the temperature-dependent SOC formation (photosynthesis) and decomposition (microbial activities and substrate decomposability) processes. The results also suggested that the large SOC stocks distributed in the low-temperature areas might increase under global warming while the small SOC stocks found in the high-temperature areas might decrease accordingly. Although it remains unknown whether the potential increasing soil carbon stocks in the low-temperature areas can offset the loss of carbon stocks in the high-temperature areas, the location- and scale- specific correlations between SOC and temperature should be taken into account for modeling SOC dynamics and SOC sequestration management.

1. Introduction

Soil serves as a nexus to produce food, fiber, and fresh water, contribute to energy and climate sustainability, and to maintain the biodiversity of the ecosystem. Much research has been conducted to understand variations in soil organic carbon (SOC) at various spatial scales and its temporal dynamics (Arrouays et al., 2012; Stockmann et al., 2015; Zhang et al., 2016; Pan et al., 2010). These studies are important not only because SOC is one of the key indices for soil quality and fertility (Stockmann et al., 2015), but also because soil acts as a carbon sink that may be able to offset increasing atmospheric CO_2 under global warming (Davidson & Janssens, 2006).

* Corresponding author.
E-mail address: budiman.minasny@sydney.edu.au (B. Minasny).

https://doi.org/10.1016/j.scitotenv.2017.09.136
0048-9697/

However, an agreement has not been reached on whether positive or negative feedback occurs between ambient/soil temperature and soil carbon stocks (Stockmann et al., 2013; McDaniel et al., 2017). From the perspective of thermodynamics, the feedback is difficult to understand because soil organic compounds with varying kinetic properties exhibit different intrinsic temperature sensitivity of decomposition due to microbial activities and other environmental constraints (e.g. soil moisture) may obscure the temperature sensitivity (Davidson & Janssens, 2006). From the perspective of sampling design, experiments monitoring soil carbon sequestration may contain large uncertainty due to the strong variability of SOC in space and time (Buma and Barrett, 2015; McDaniel et al., 2017). More importantly, variations in soil properties and their inter-relationship with environmental factors can be location- and scale- specific (Lark et al., 2004; Hu and Si, 2013; O'Rourke et al., 2015; Zhou et al., 2016; Huang et al., 2017), which is often overlooked in the agro-ecosystem models for SOC simulations (Brilli et al., 2017).

To deal with the spatio-temporal variations in SOC, the digital soil mapping approach can be potentially useful. This requires coupling easy-to-obtain ancillary data with a relatively small number of soil samples to predict soil properties and types at large spatial scales using non-spatial/spatial models (McBratney et al., 2003). Recently, maps of SOC have been generated across the world with high spatial resolution (i.e. 250 m–1 km) and acceptable accuracy (Stockmann et al., 2015; Hengl et al., 2017; Minasny et al., 2017). To extract the location- and scale-specific variations in SOC and soil temperature, various scale analysis methods may be employed (Lark et al., 2004; Hu and Si, 2013).

In this study, a spherical scale-discretised wavelet analysis algorithm (Leistedt et al., 2013) was employed to extract the location- and scale-specific variations in global SOC (Stockmann et al., 2015) at two depths (i.e. 0–5 cm and 30–60 cm) and used to understand the location- and scale- specific correlation between temperature and SOC sequestration across the globe. Although it was possible to study the location- and scale- specific correlation between other environmental variables and SOC, we would not explore this issue in the paper. This was because our preliminary analysis unveiled that there were no contrasting patterns (i.e. positive or negative) of the location- and scale- specific correlations between other environmental variables (e.g. precipitation) and SOC as compared to that between temperature and SOC.

2. Materials and methods

2.1. Data collection and standardisation

The global maps of soil organic matter (SOC) used in this study have been previously reported by Stockmann et al. (2015). In brief, 94,381 soil profiles collected mostly between 1960 and 2010 around the world were used for data mining along with a number of environmental covariates including digital elevation models and their derivatives, climate data (long-term precipitation and temperature data), and land cover data. The locations of the soil profiles were shown in Stockmann et al. (2015). The data mining modeling and mapping processes were conducted using the Google Earth Engine platform Padarian et al. (2015). To evaluate the mapping uncertainty, a quasi-automatic bootstrapping algorithm was used which randomly selected points for training the classifiers (Padarian et al., 2015). Herein, 10 simulations were carried out to obtain SOC maps across the globe and calculate the 90% confidence interval.

The global digital elevation model (DEM) was obtained from WorldGrids (2017). It was calculated using SRTM 30+ and ETOPO DEM at 30 arc-seconds. The global maps of mean land surface temperature and precipitation were calculated using the average monthly climate data (WorldClim version 2) for 1970–2000 at 30 arc-seconds (Hijmans et al., 2015). The global map of land surface temperature predicted in 2100 was calculated using the mean values of maximum and minimum land surface temperature at 0.25 arc-degrees estimated in 2100 under the rcp45 scenario using the CCSM4 model. The data layers were obtained from NASA (2017).

The mean land surface temperature (long term mean during 1970–2000 and prediction in 2100) was used as soil temperature at 0–5 cm. Soil temperature at 30–60 cm was estimated using the corresponding land surface temperature and soil thermal properties (thermal conductivity and heat capacity). The global maps of soil thermal conductivity and heat capacity were obtained from global soil datasets for Earth system modeling (http://globalchange.bnu.edu.cn/research/soil4.jsp) at 30 arc-seconds (Shangguan et al., 2014).

The global map of vegetation index and phenology (VIP) was obtained from Land Processes Distributed Active Archive Center. The VIP collections were based on Moderate Resolution Imaging Spectroradiometer (MODIS), Advanced Very High Resolution Radiometer (AVHRR), and Satellite Pour l'Observation de la Terre (SPOT) data inputs (Didan, 2016). The global map of soil clay content (0–5 cm) was obtained from ISRIC-World Soil Information (Hengl et al., 2017).

Because the climate data used were the long-term average values (1970–2000) and the SOC data (1960–2010) were collected at different times, it was assumed that the predicted SOC represented the average SOC during 1970–2000. Given the resolution of the ancillary data used to estimate SOC (e.g. 30 arc-seconds) and the potential noises of the data at the local scales, all the maps were resampled onto a grid of 0.0898 arc-degrees (approximately 10 km at the equator) using the nearest-neighbour algorithm.

2.2. Scale-discretised wavelet transform on the sphere

Wavelet transform uses a certain type of wavelet and corresponding scaling functions as the basis to decompose a set of data into components described by wavelet coefficients, which are specific to spatial scales and locations (Lark et al., 2004). Particularly, the scale-discretised wavelet transform can separate variations in soil properties at some pre-selected scales (Percival, 1995), which is equivalent to inspecting specimens using a microscope with different lenses.

Wavelet transform can be applied on a plane or a sphere. To investigate the scales of the soil variations across the globe, the Matlab package S2LET (Leistedt et al., 2013) was used to conduct spherical scale-discretised wavelet transform for the maps of SOC (0–5 cm and 30–60 cm), and temperature (1970–2000 and 2100) (0–5 cm and 30–60 cm). The wavelets used in the study were constructed through a tiling of the harmonic line following Leistedt et al. (2013). This type of wavelets can be used to probe spatially localised, scale-dependent features of signals (e.g. SOC and temperature) on the sphere (McEwen et al., 2005). In this study, the MW sampling scheme was used to obtain a theoretically exact transform (McEwen and Wiaux, 2011).

The scaling parameter of the wavelet functions (i.e. λ) was set to 3 and the lowest and highest scales of the wavelet decomposition were set to 2 and 7, respectively. The λ value was selected so that the levels of decomposition were neither too few nor too many. This would generate 6 wavelet coefficients at level (i) 2 to 7 (i.e. C2–C7), representing the spatial scales of ($180/3^{i-1}$, $180/3^{i+1}$) arc-degrees (Leistedt et al., 2013). For example, the wavelet coefficient at the coarsest scale (i.e. C2) had the support of (6.7°, 60°) while the wavelet coefficient at the finest scale (i.e. C7) had the support of (0.03°, 0.25°).

The variance of wavelet coefficient at each level i (Var_i) was calculated using the following formula (Percival, 1995):

$$Var_i = \frac{1}{3^i N_i} \sum_{n=1}^{N_i} W_{i,n}^2 \quad (1)$$

where N_i is the number of measurements across the globe and $W_{i,n}$ is the n_{th} wavelet coefficient at level i.

Then the percentage of wavelet coefficient to the total variance (Percentage of Var_i) was calculated as follows:

$$\text{Percentage of } Var_i = \frac{Var_i}{\sum_{i=2}^{7} Var_i} \times 100 \quad (2)$$

2.3. Calculating the scale- and location-specific Pearson's correlation coefficient

The localised spatial Pearson's correlation coefficients between the corresponding wavelet components (e.g. C1 of SOC and C1 of DEM) were calculated using a moving window of 15 by 15 points. The radius was empirically selected so that the number of data points were neither too few (i.e. not statistically significant) nor too many (i.e. costing too much computation time and failing to account for the local variations). For example, if window size was set as 5 by 5, 25 points were included for calculating the Pearson's correlation coefficient, whereby the significance may be misleading (Hewitt et al., 2016). By comparison, when the window size was 25 by 25, 625 points were used, which may not represent the local variations of SOC. When the window size was set as 15 by 15, 225 points were used to calculate the localised correlation coefficients, with $r > 0.5$) and $r < -0.5$ indicating two-tailed P value < 0.0001.

3. Results and discussion

3.1. Spatial distribution of SOC across the globe

The spatial distribution of predicted SOC at 0–5 cm was presented across the globe (Fig. 1a). Large SOC content (>6.4%) was mostly located in the arctic zones and in the high mountain ranges (e.g. Himalayas, Andes, Alps). Conversely, small SOC values (<0.8%) were found in the arid areas (e.g. Sahara, central Australia, west of the USA). In addition, intermediate SOC values (1.6–3.2%) were found in various regions associated with tropical rain forests although carbon decomposition in these areas was active due to strong microbiological activities. This was in agreement with the previous studies (Brown and Lugo, 1982; Donato et al., 2011). Predicted SOC at 30–60 cm showed a similar pattern but the values were smaller than that at 0–5 cm (Fig. 1b). The 90% confidence intervals of the predicted SOC were presented in Fig. 1c and Fig. 1d. Given that the confidence intervals were <5% and 1% for most parts of the world at 0–5 cm and 30–60 cm, respectively, these maps of predicted SOC were considered accurate.

3.2. Spatial distribution of wavelet coefficients of SOC across the globe

The location- and scale- specific variations in SOC at the depth of 0–5 cm were represented by various wavelet coefficients (i.e. C2–C7) (Fig. 2). The spatial supports of these coefficients decreased from C2 to C7 (Table 1). It was found that the distribution of the scale-specific variations in SOC across the globe was consistent with the classical "CLORPT" model (Jenny, 1994), which described soil genesis as a function of climate (CL), organism (O), relief (R), parent materials (P) and time (T). Similar patterns of the spatial distribution of wavelet coefficient were also identified for SOC at the depth of 30–60 cm (results not shown). Herein, we describe the coefficients of SOC (0–5 cm) from the largest spatial scale to the smallest spatial scale.

At the scale of C2 (i.e. continental scale), the spatial distribution of SOC values was mainly controlled by climate factors (i.e. temperature

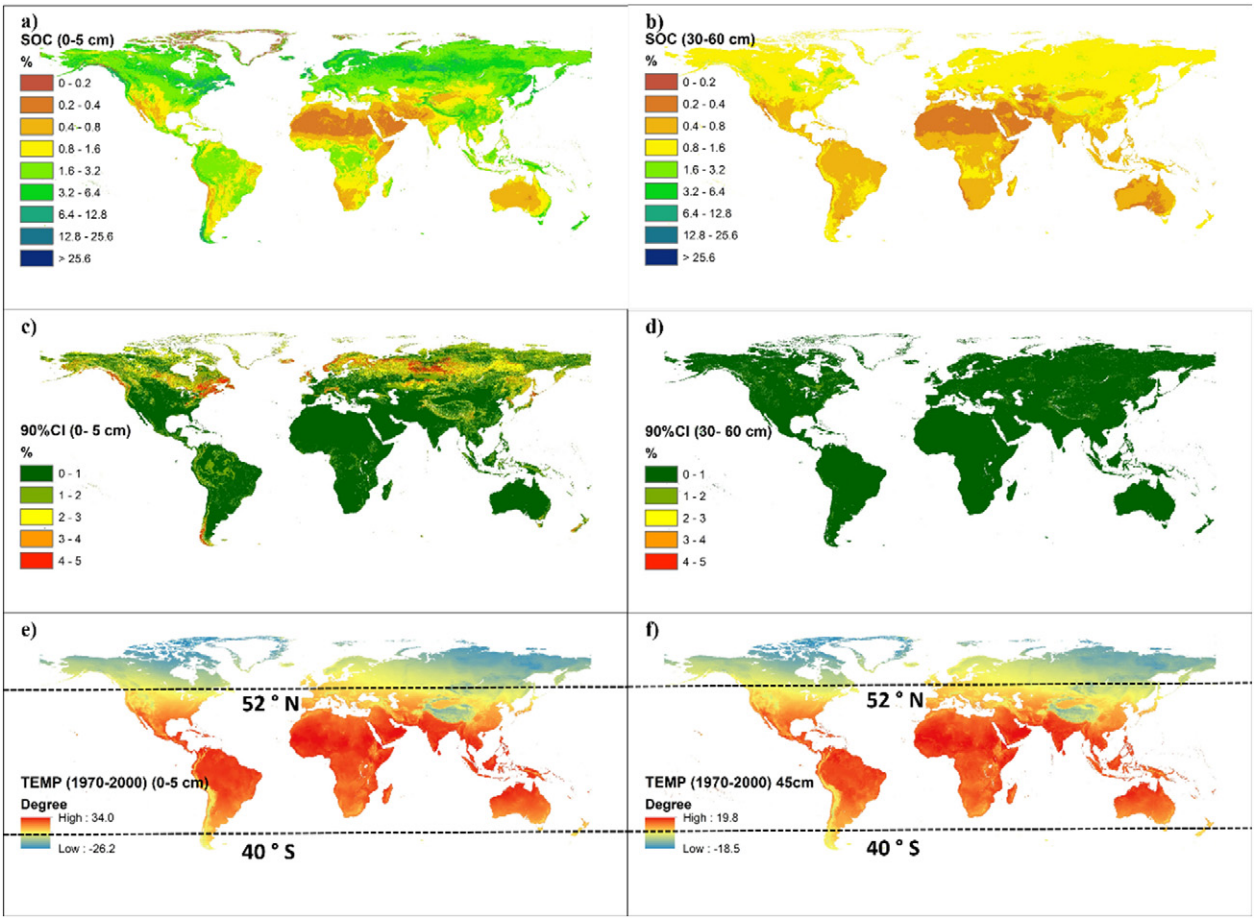

Fig. 1. Spatial distribution of soil organic carbon (SOC) at a) 0–5 cm and b) 30–60 cm, and 90% confidence interval (CI) of predicted SOC at the depths of c) 0–5 cm and d) 30–60 cm, and long-term average soil temperature (1970–2000) at e) 0–5 cm and f) 30–60 cm, respectively.

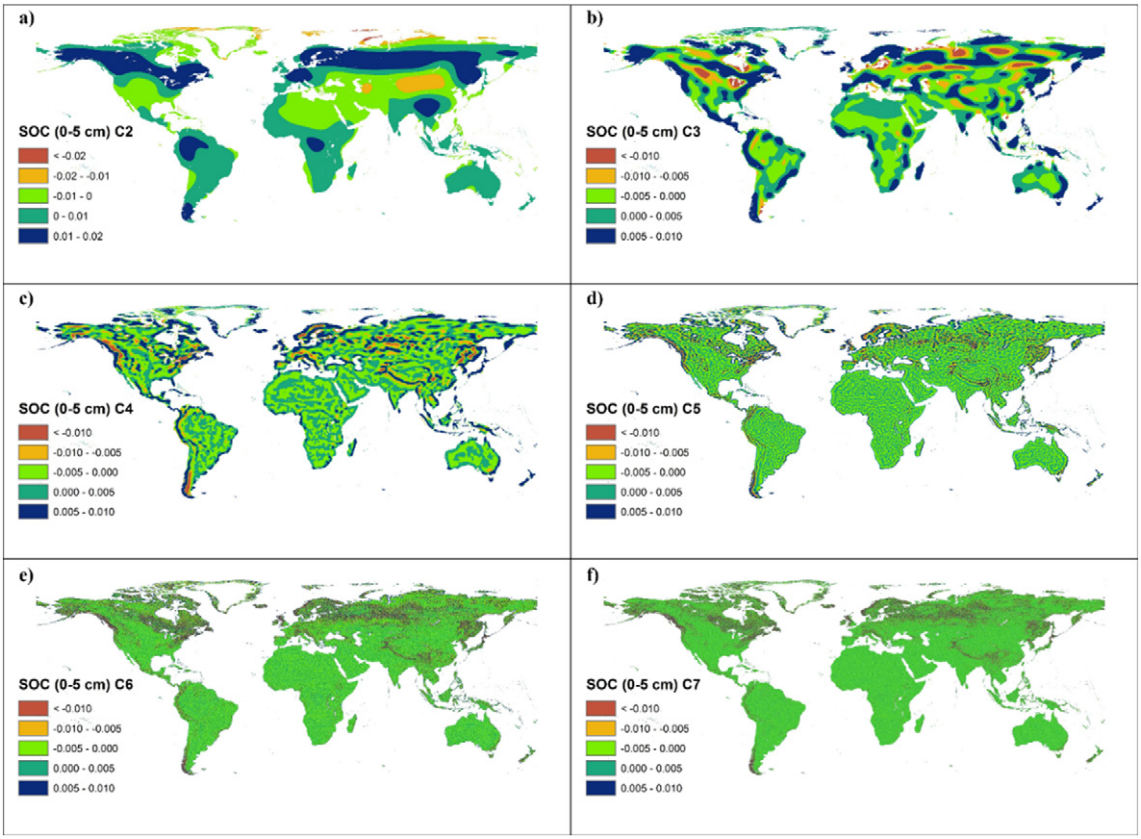

Fig. 2. Spatial distribution of the wavelet coefficients of soil organic carbon (SOC) at 0–5 cm and at various levels, including a) C2, b) C3, c) C4, d) C5, e) C6, and f) C7, respectively.

and precipitation, refer to Fig. 1e and Fig. 3b, respectively). For example, large SOC wavelet coefficient values (0.01–0.02) were identified in the subarctic region and tropical forests mainly due to low carbon decomposition and high net primary production, respectively. Conversely, low (<−0.02) and intermediate-low (−0.02) SOC wavelet coefficient values were located in the arctic regions and the arid Mongolian plateau due to low net primary production.

At the scale of C3 (i.e. sub-continental scale), the variation in SOC was mainly controlled by organisms (represented by different vegetation and land cover types) (Fig. 3e), parent materials (see Fig. 3d), and elevation (Fig. 3a). For example, large (>0.005) and small (<−0.010) SOC wavelet coefficient alternated from west to east across central Russia most likely due to the changing vegetation types (Fig. 3e) and parent materials (Fig. 3d). In isolated regions where the elevation was high, such as the Himalayan, Rocky, Andes, and Alps Mountains, large SOC wavelet coefficient was also evident.

At the scale of C4 (i.e. national scale), the distribution of SOC was also controlled by relief. This indicated that one soil forming factor can have an impact on the spatial variation in SOC at different spatial scales. This was also confirmed by previous studies (Huang et al., 2015; Zhou et al., 2016). At the finer scales (i.e. C5–C7), the variations in SOC were minimal and only accounted for ~1.5% of the total variance of SOC (Table 1). These variations can be attributed to either the small-scale variation in SOC or the noises in the environmental covariates used to estimate SOC such as land cover (see Fig. 3e).

Table 1
Spatial supports of the various wavelet coefficients of soil organic carbon (0–5 cm) and their percentage of the total variance.

Wavelet coefficients	Spatial support on the sphere (arc-degree)	Approximate spatial scales	Percentage of the total variance (%)
C2	6.67–60.00	continental	78.0
C3	2.22–20.00	sub-continental	15.9
C4	0.74–6.67	national	4.6
C5	0.25–2.22	regional	1.0
C6	0.08–0.74	catchment	0.4
C7	0.03–0.25	local	0.1

3.3. Location- and scale- specific correlations between SOC and temperature

Fig. 4a–e show the spatial distribution of localised Pearson's r between various wavelet coefficients of SOC and the corresponding wavelet coefficients of temperature (1970–2000) at 0–5 cm. The correlation coefficient at the scale of C5 was particularly worth noting (Fig. 4d). Between 52° N and 40° S, SOC was negatively correlated with soil temperature. In these tropical and temperate zones, the soil temperature is the dominant limiting factor of soil respiration (SOC decomposition), whereas photosynthesis (SOC formation) is limited by multiple factors, including light, CO_2 concentration, water stress, and nutrient availability (Stockmann et al., 2013; Ouyang et al., 2016). Therefore, this negative correlation was most likely due to the increasing soil respiration with increasing temperature (Post et al., 1982; Ghosh et al., 2016). Similar negative correlations were also identified in these tropical and temperate zones at other spatial scales (i.e. C2–C7). This was consistent with most of the studies that concluded soil carbon decomposition increased more with increasing temperature than did the net primary productivity (Kirschbaum, 2000; Nemani et al., 2003; Gao et al., 2013; Selmants et al., 2014; Bragazza et al., 2016; Soleimani et al., 2017).

However, to the north of 52° N and south of 40° S, SOC was positively correlated with soil temperature. In these arctic zones, the positive correlation was probably due to the fact that SOC decomposition was strongly inhibited by the low temperature while net primary production increased significantly with increasing soil temperature (Ghosh et al., 2016; Nemani et al., 2003; Gao et al., 2013; McGuire et al., 2016). The positive correlation was consistent with Liski et al. (1999), who

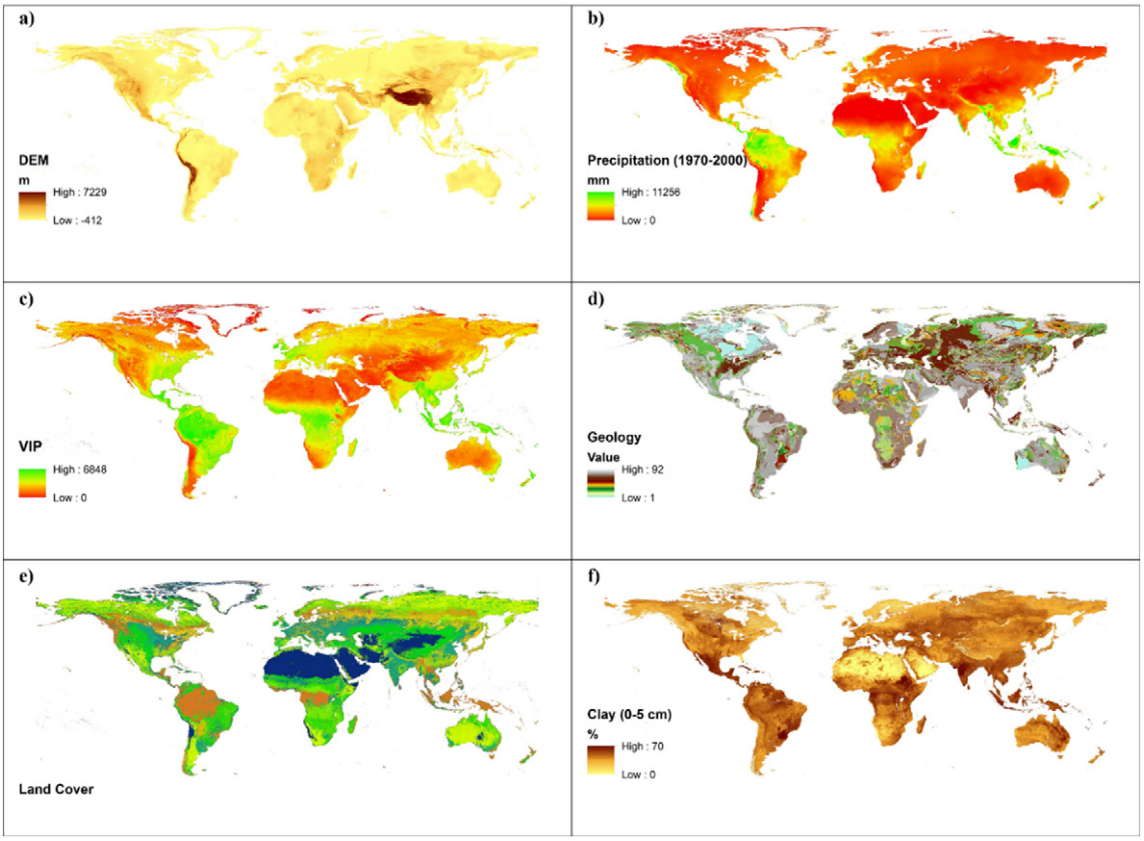

Fig. 3. Spatial distribution of various environmental factors across the globe, including a) digital elevation model (DEM), b) long-term average annual precipitation during 1970–2000, c) vegetation index and phenology (VIP), d) surface geological units, e) land cover types and f) predicted clay content at 0–5 cm.

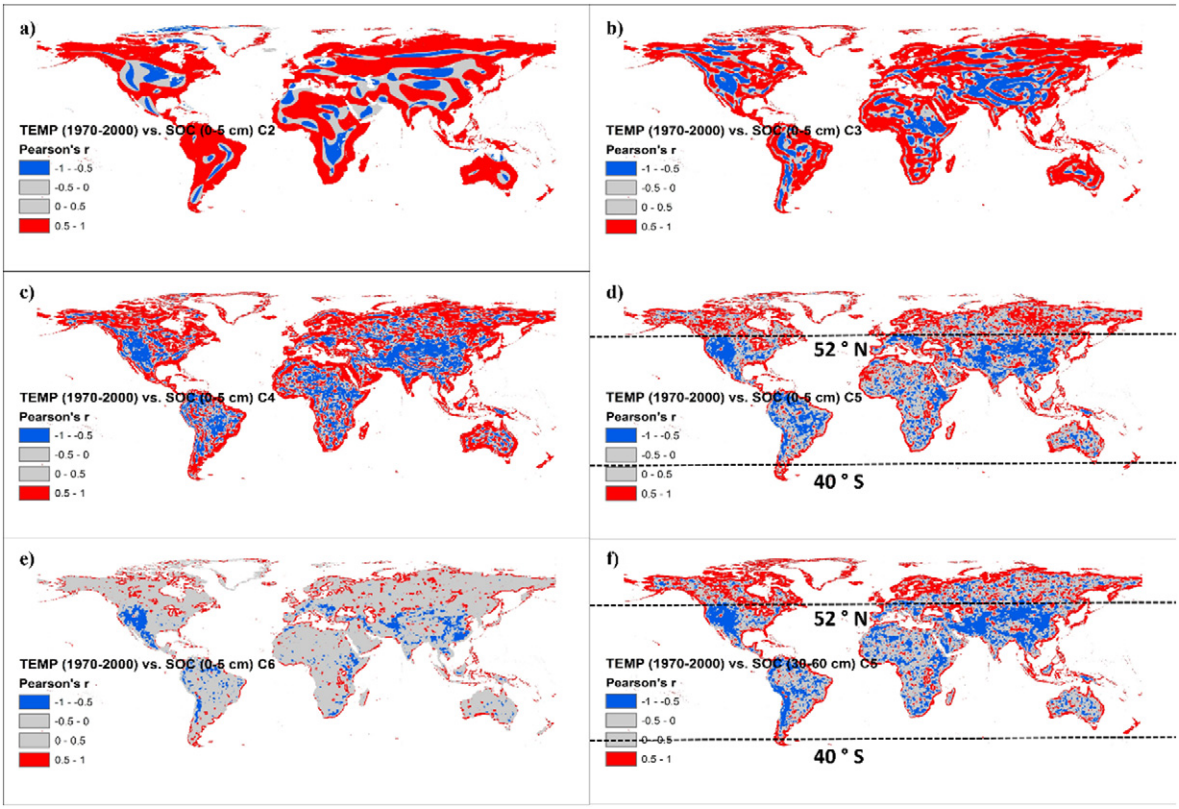

Fig. 4. Spatial distribution of localised Pearson's correlation coefficients between the wavelet coefficients of soil organic carbon (SOC) at 0–5 cm and long-term average soil temperature at 0–5 cm during 1970–2000, including a) coefficient 2 (C2), b) coefficient 3 (C3), c) coefficient 4 (C4), d) coefficient 5 (C5), e) coefficient 6 (C6), and f) between coefficient 5 (C5) of SOC and long-term average (1970–2000) soil temperature at 30–60 cm.

found that old soil organic matter (i.e. >9, 000 years) in Finland was resistant to changes in temperature and suggested that soil carbon storage of boreal forest soils would increase during global warming. The positive correlation was also consistent with McGuire et al. (2016) who modelled that both vegetation and soil carbon storage together have increased by 156 to 954 TgC yr^{-1} between 1960 and 2009 over the permafrost region in the northern hemisphere under global warming.

The positive correlation could also be caused by the shift in microbial communities and vegetation with temperature (Ågren, 2000; Leblans et al., 2017; Wang et al., 2017; Yu et al., 2017), the elongated length of the growing season and genetic adaptations (Leblans et al., 2017), and changes in environmental constraints of carbon decomposition (Stockmann et al., 2013) including precipitation, land cover, management practices, and clay content (refer to Fig. 3 for their spatial distributions).

Similar patterns of positive and negative correlations were identified at the depth of 30–60 cm (Fig. 4f). This suggested that at the regional scale (i.e. C5), the large SOC stocks distributed in the low-temperature areas would increase under global warming while the small SOC stocks found in the high-temperature areas would decrease accordingly.

3.4. Temperature sensitivity of SOC sequestration

To further understand the temperature sensitivity of SOC sequestration, the correlation between wavelet coefficient 5 (C5) of SOC and soil temperature at 0–5 cm were plotted against different soil temperature zones (Fig. 5). Based on the plot of untransformed SOC versus soil temperature, it was difficult to identify any significantly positive or negative correlations (Fig. 5a). This suggested the reason why some studies identified no correlations between SOC and temperature (Davidson & Janssens, 2006; Stockmann et al., 2013). However, when inspecting the correlation at certain spatial scales (e.g. C5), SOC was found strongly positively correlated with soil temperature ($R^2 = 0.33$, $P < 0.001$) when soil temperature was lower than 0 °C (Fig. 5b). This temperature domain was mostly found in arctic zones and high mountain ranges and it can be concluded that increase in soil temperature had a greater impact on SOC formation than decomposition at 0–5 cm. This was maybe because cold temperature acted as an environmental constraint (i.e. presence of permafrost) which inhibited SOC decomposition (Davidson & Janssens, 2006) while increasing temperature greatly induced SOC formation via elongating the length of the growing season and genetic adaptations as well as shifting the microbial communities (Ågren, 2000; Leblans et al., 2017).

Conversely, when soil temperature was higher than 10 °C, the correlation became slightly positive (Fig. 5d), which was masked by the negative correlation between SOC and soil temperature occurring in the various places (Fig. 4d). This temperature domain was mainly found in tropical/temperate zones and the result suggested that increase in soil temperature in these areas had a non-significant impact on SOC sequestration within 0–5 cm. Interestingly, between 0 °C and 10 °C, two types of correlations were identified (Fig. 5c), corresponding to those identified at the low-temperature (<0 °C) or high-temperature domains

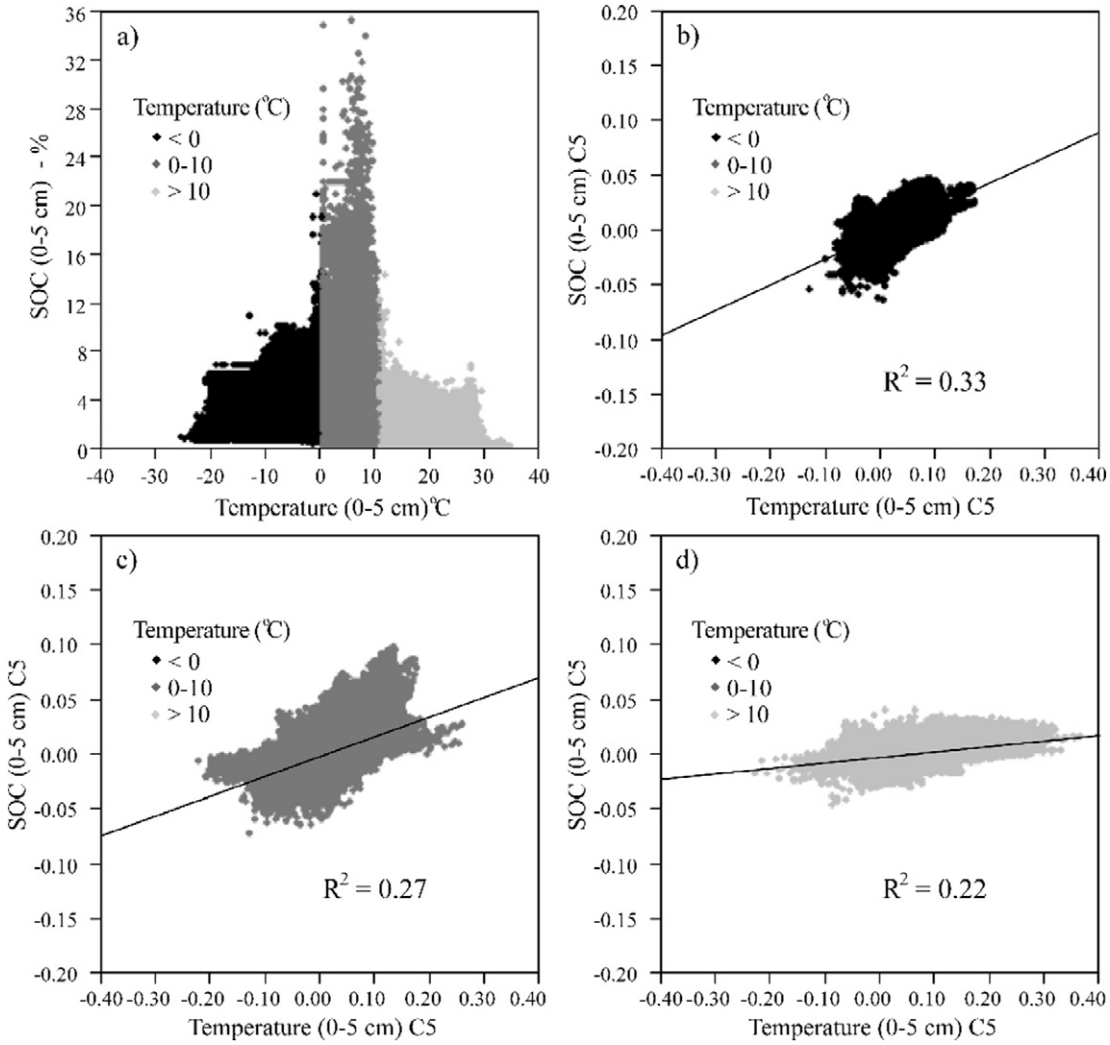

Fig. 5. Plots of a) soil organic carbon (SOC) versus long-term average soil temperature (1970–2000), and b) to d) wavelet coefficient 5 (C5) of SOC versus C5 of soil temperature at 0–5 cm.

(>10 °C). This narrow temperature domain (0–10 °C) suggested the temperature sensitivity of SOC sequestration at 0–5 cm, which was a result of interactions between different temperature-dependent factors associated carbon decomposition and photosynthesis (Davidson & Janssens, 2006).

The temperature sensitivity of SOC sequestration at the scale of C5 was also identified at the depth of 30–60 cm (Fig. 6). Similarly, when soil temperature was lower than −5 °C, SOC was positively correlated with soil temperature ($R^2 = 0.80$, $P < 0.001$) (Fig. 6b). Conversely, when soil temperature was higher than 5 °C, the correlation was only slightly positive (Fig. 6d) and was masked by the negative correlation between SOC and soil temperature occurring at various places (Fig. 4f). Similarly, between −5 °C and 5 °C, two types of correlations were identified (Fig. 6c), suggesting the coexistence of SOC decomposition and formation processes.

It was also noted that the temperature domains for the coexistence of SOC decomposition and formation were different at different depths. This may be caused by varying soil organic compounds with depth, such as decadally cycling and fast cycling soil carbon (Lin et al., 2015). These compounds have different substrate decomposability, such as carbon-to nitrogen ratios and lignin contents (Meentemeyer, 1978; Melillo et al., 1982; Feng et al., 2015) and are susceptible to depth-varying environmental constraints such as physical and chemical protection from carbon decomposition including soil moisture and aggregates (Davidson & Janssens, 2006; Feng et al., 2015; Ding et al., 2016).

3.5. Potential impacts of global warming on SOC sequestration

The positive correlation between SOC and soil temperature in the low-temperature areas suggests SOC may increase as a result of global warming in the arctic areas and high mountain ranges where SOC is relatively large (Fig. 4d and Fig. 1a). As the change in soil temperature is smaller at depths (e.g. 30–60 cm), the increase in SOC at depths in the low-temperature areas might be minimal under global warming.

However, it should be noted that the areas in which SOC and soil temperature are positively correlated may shrink with increasing soil temperature during global warming as illustrated by one of the global temperature projections in 2100 (see Fig. 7). It is envisaged that the boundaries (i.e. 52° N parallel and 40° S parallel) would shift northward and southward when soil temperature increases, respectively.

In addition, it remains unknown whether the location- and scale-specific temperature effect on soil carbon sequestration will produce net CO_2 efflux or influx because the overall net primary productivity in the arctic areas and high mountain ranges is very low compared to the tropical and temperate zones (as illustrated by the vegetation index and phenology in Fig. 3c).

4. Conclusions

It can be concluded that the correlation between SOC and soil temperature can be positive or negative across the world, depending on

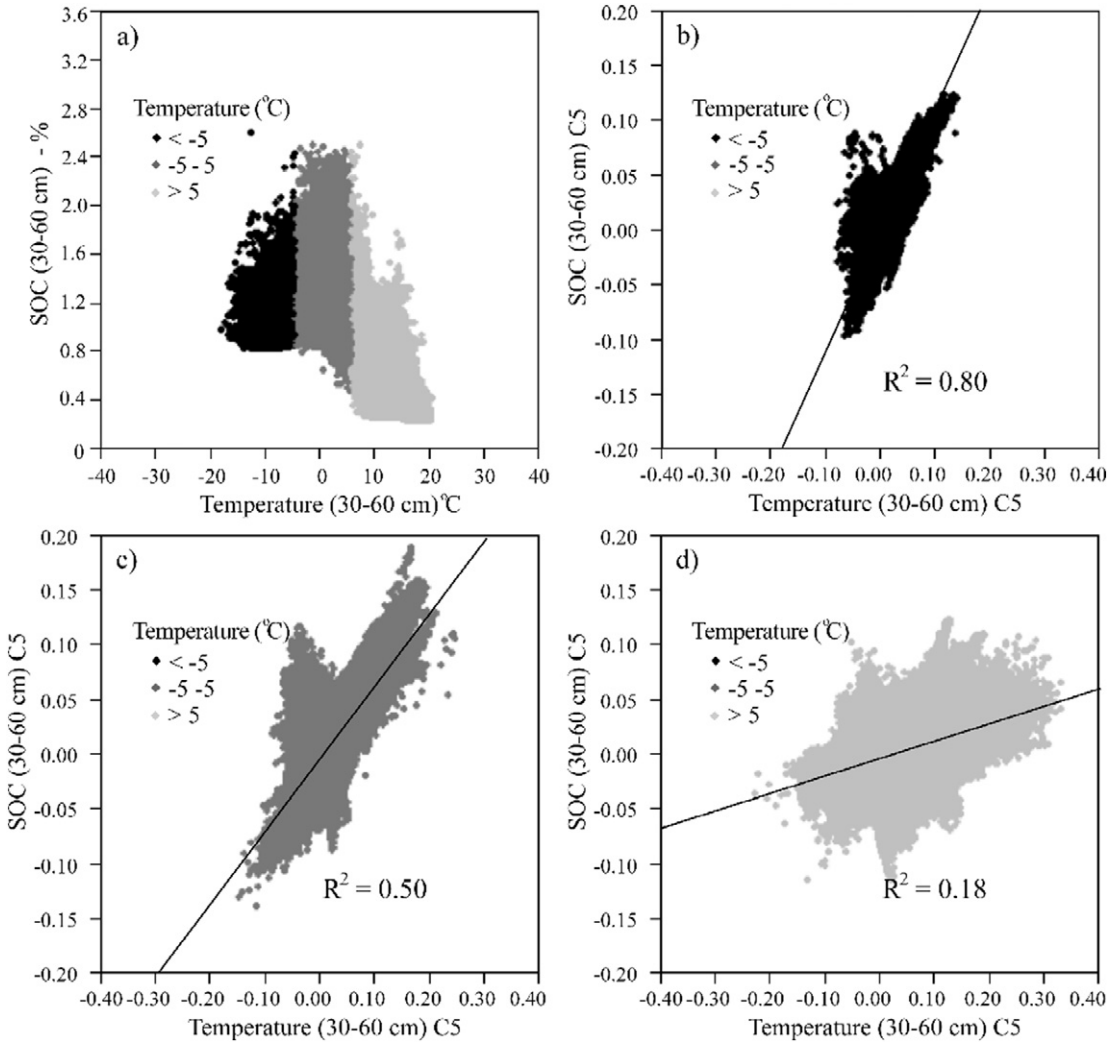

Fig. 6. Plots of a) soil organic carbon (SOC) versus long-term average soil temperature (1970–2000), and b) to d) wavelet coefficient 5 (C5) of SOC versus C5 of soil temperature at 30–60 cm.

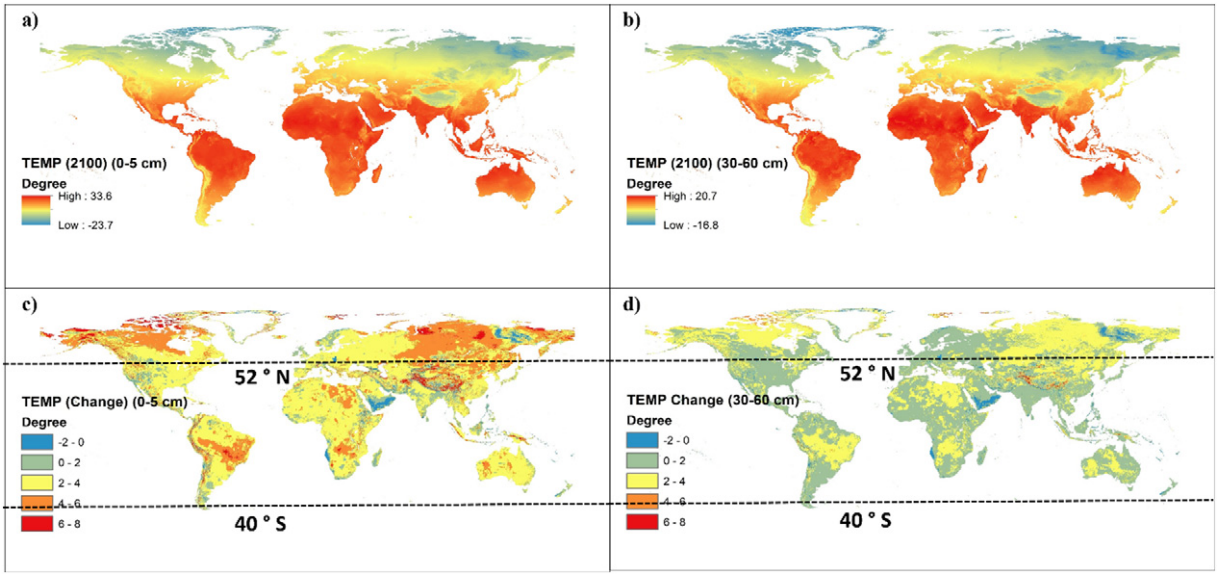

Fig. 7. Spatial distribution of soil temperature predicted in 2100 at a) 0–5 cm and b) 30–60 cm and change in soil temperature from 1970 to 2000 to 2100 at c) 0–5 cm and d) 30–60 cm, respectively.

the locations and scales. SOC may increase as a result of global warming in the arctic areas and high mountain ranges where SOC is relatively large. Additionally, current SOC dynamics models may need to be revised to account for the location- and scale- specific correlations between SOC and soil temperature, particularly in the arctic zones and high mountain ranges (Miller et al., 2016). This has been overlooked in the past due to the limited soil sampling data collected in these areas (Davidson & Janssens, 2006; Stockmann et al., 2013).

From the perspective of soil carbon sequestration, different management practices could be applied by taking into account the scale- and location- specific correlations between SOC and temperature, as well as other environmental factors such as elevation, precipitation, land cover, and land use (Houghton et al., 2012). In the arctic zones and high mountain ranges, priority should be given to the protection of biodiversity in the uplands and tropical rain forest to maintain the large soil carbon stocks. In the tropical and temperate zones, management practices should be applied to avoid soil erosion and loss (Lal, 1990) and adopt conservation farming (Blanco-Canqui and Lal, 2008).

Acknowledgements

The authors acknowledged Dr. Boris Leistedt (New York University) and Professor Jason McEwen (University College London) for their guidance with the implementation of the Matlab package S2LET. The authors also acknowledged Associate Professor Wei Shangguan (Sun Yat-Sen University) for providing the global datasets of soil thermal conductivity and thermal capacity. Budiman Minasny and Alex B. McBratney acknowledged the funding from ARC Discovery Project DP140102283: A general soil spatial scaling theory. The authors declared that there was no conflict of interest or relationship, financial or otherwise, that might influence authors' objectivity on the paper. The global soil carbon maps and the wavelet analysis codes can be obtained by contacting the corresponding author.

References

Ågren, G.I., 2000. Temperature dependence of old soil organic matter. Ambio 29, 55.
Arrouays, D., Marchant, B.P., Saby, N.P.A., Meersmans, J., Orton, T.G., Martin, M.P., Bellamy, P.H., Lark, R.M., Kibblewhite, M., 2012. Generic issues on broad-scale soil monitoring schemes: a review. Pedosphere 22, 456–469.
Blanco-Canqui, H., Lal, R., 2008. No-tillage and soil-profile carbon sequestration: an on-farm assessment. Soil Sci. Soc. Am. J. 72, 693–701.
Bragazza, L., Buttler, A., Robroek, B.J.M., Albrecht, R., Zaccone, C., Jassey, V.E.J., Signarbieux, C., 2016. Persistent high temperature and low precipitation reduce peat carbon accumulation. Glob. Chang. Biol. 22, 4114–4123.
Brown, S., Lugo, A.E., 1982. The storage and production of organic matter in tropical forests and their role in the global carbon cycle. Biotropica 14, 161–187.
Buma, B., Barrett, T.M., 2015. Spatial and topographic trends in forest expansion and biomass change, from regional to local scales. Glob. Chang. Biol. 21, 3445–3454.
Davidson, E.A., Janssens, I.A., 2006. Temperature sensitivity of soil carbon decomposition and feedbacks to climate change. Nature 440 (7081), 165.
Didan, K.A.B., 2016. NASA Measures Vegetation Index and Phenology (VIP) Phenology EVI2 Yearly Global 0.05Deg CMG (Data set). NASA EOSDIS Land Processes DAAC. (Data available from). https://lpdaac.usgs.gov/V4/VI_PHENOLOGY/.
Ding, J., Chen, L., Zhang, B., Liu, L., Yang, G., Fang, K., Chen, Y., Li, F., Kou, D., Ji, C., Luo, Y., Yang, Y., 2016. Linking temperature sensitivity of soil CO2 release to substrate, environmental, and microbial properties across alpine ecosystems. Glob. Biogeochem. Cycles 30, 1310–1323.
Donato, D.C., Kauffman, J.B., Murdiyarso, D., Kurnianto, S., Stidham, M., Kanninen, M., 2011. Mangroves among the most carbon-rich forests in the tropics. Nat. Geosci. 4, 293–297.
Feng, X., Gustafsson, Ö., Holmes, R.M., Vonk, J.E., van Dongen, B.E., Semiletov, I.P., Dudarev, O.V., Yunker, M.B., Macdonald, R.W., Wacker, L., Montluçon, D.B., Eglinton, T.I., 2015. Multimolecular tracers of terrestrial carbon transfer across the pan-Arctic: 14C characteristics of sedimentary carbon components and their environmental controls. Glob. Biogeochem. Cycles 29, 1855–1873.
Gao, Y., Zhou, X., Wang, Q., Wang, C., Zhan, Z., Chen, L., Yan, J., Qu, R., 2013. Vegetation net primary productivity and its response to climate change during 2001–2008 in the Tibetan plateau. Sci. Total Environ. 444, 356–362.
Ghosh, A., Bhattacharyya, R., Dwivedi, B.S., Meena, M.C., Agarwal, B.K., Mahapatra, P., Shahi, D.K., Salwani, R., Agnihorti, R., 2016. Temperature sensitivity of soil organic carbon decomposition as affected by long-term fertilization under a soybean based cropping system in a sub-tropical Alfisol. Agric. Ecosyst. Environ. 233, 202–213.
Hengl, T., de Jesus, J.M., Heuvelink, G.B.M., Gonzalez, M.R., Killibarda, M., Blagotic, A., Shangguan, W., Wright, M.N., Geng, X., Bauer-Marschallinger, B., Guevara, M.A., Vargas, R., MacMillan, R.A., Batjes, N.H., Leenaars, J.G.B., Ribeiro, E., Wheeler, I., Mantel, S., Kempen, B., 2017. SoilGrids250m: global gridded soil information based on machine learning. PLoS One 12, e0169748.
Hewitt, C.L., Campbell, M.L., Davidson, A.D., 2016. Deciphering P values: beware false certainty. Science 353, 551.
Hijmans, R.J., Cameron, S., Parra, J., Jones, P.G., Jarvis, A., Richardson, K., 2015. WorldClim-global Climate Data. Free Climate Data for Ecological Modeling and GIS. (Data available from). http://worldclim.org/version2.
Houghton, R.A., House, J.I., Pongratz, J., van der Werf, G.R., DeFries, R.S., Hansen, M.C., Le Quéré, C., Ramankutty, N., 2012. Carbon emissions from land use and land-cover change. Biogeosciences 9, 5125–5142.
Huang, J., Shi, Z., Biswas, A., 2015. Characterizing anisotropic scale-specific variations in soil salinity from a reclaimed marshland in China. Catena 131, 64–73.
Huang, J., Wu, C., Minasny, B., Roudier, P., McBratney, A.B, 2017. Unravelling scale-and location-specific variations in soil properties using the 2-dimensional empirical mode decomposition. Geoderma 307, 139–149.
Hu, W., Si, B.C., 2013. Soil water prediction based on its scale-specific control using multivariate empirical mode decomposition. Geoderma 193, 180–188.
Jenny, H., 1994. Factors of Soil Formation: A System of Quantitative Pedology. Courier Corporation.

Kirschbaum, M.U., 2000. Will changes in soil organic carbon act as a positive or negative feedback on global warming? Biogeochemistry 48, 21–51.
Lal, R., 1990. Soil Erosion in the Tropics: Principles and Management. McGraw-Hill Inc.
Lark, R.M., Milne, A.E., Addiscott, T.M., Goulding, K.W.T., Webster, C.P., O'Flaherty, S., 2004. Scale- and location- dependent correlation of nitrous oxide emissions with soil properties: an analysis using wavelets. Eur. J. Soil Sci. 55, 611–627.
Leblans, N.I., Sigurdsson, B.D., Vicca, S., Fu, Y., Penuelas, J., Janssens, I.A., 2017. Phenological responses of Icelandic subarctic grasslands to short-term and long-term natural soil warming. Glob. Chang. Biol. (in press). https://doi.org/10.1111/gcb.13749.
Leistedt, B., McEwen, J.D., Vandergheynst, P., Wiaux, Y., 2013. S2LET: a code to perform fast wavelet analysis on the sphere. Astron. Astrophys. 558, A128.
Lin, J., Zhu, B., Cheng, W., 2015. Decadally cycling soil carbon is more sensitive to warming than faster-cycling soil carbon. Glob. Chang. Biol. 21, 4602–4612.
Liski, J., Ilvesniemi, H., Mäkelä, A., Westman, C.J., 1999. CO_2 emissions from soil in response to climatic warming are overestimated: the decomposition of old soil organic matter is tolerant of temperature. Ambio 28, 171–174.
McBratney, A.B., Santos, M.M., Minasny, B., 2003. On digital soil mapping. Geoderma 117, 3–52.
McDaniel, M.D., Simpson, R.G., Malone, B.P., McBratney, A.B., Minasny, B., Adams, M.A., 2017. Quantifying and predicting spatio-temporal variability of soil CH4 and N2O fluxes from a seemingly homogeneous Australian agricultural field. Agric. Ecosyst. Environ. 240, 182–193.
McEwen, J.D., Hobson, M.P., Lasenby, A.N., Mortlock, D.J., 2005. A high-significance detection of non-Gaussianity in the WMAP 1-year data using directional spherical wavelets. Mon. Not. R. Astron. Soc 359, 1583–1596.
McEwen, J.D., Wiaux, Y.A., 2011. A novel sampling theorem on the sphere. IEEE Trans. Signal Process. 59, 5876–5887.
McGuire, A.D., Koven, C., Lawrence, D.M., Clein, J.S., Xia, J., Beer, C., Burke, E., Chen, G., Chen, X., Delire, C., Jafarov, E., MacDougall, A.H., Marchenko, S., Nicolsky, D., Peng, S., Rinke, A., Saito, K., Zhang, W., Alkama, R., Bohn, T.J., Ciais, P., Decharme, B., Ekici, A., Gouttevin, I., Hajima, T., Hayes, D.J., Ji, D., Krinner, G., Lettenmaier, D.P., Luo, Y., Miller, P.A., Moore, J.C., Romanovsky, V., Schädel, C., Schaefer, K., Schuur, E.A.G., Smith, B., Sueyoshi, T., Zhuang, Q., 2016. Variability in the sensitivity among model simulations of permafrost and carbon dynamics in the permafrost region between 1960 and 2009. Glob. Biogeochem. Cycles 30, 1015–1037.
Meentemeyer, V., 1978. Macroclimate and lignin control of litter decomposition rates. Ecology 59, 465–472.
Melillo, J.M., Aber, J.D., Muratore, J.F., 1982. Nitrogen and lignin control of hardwood leaf litter decomposition dynamics. Ecology 63, 621–626.
Miller, S.M., Miller, C.E., Commane, R., Chang, R.Y.W., Dinardo, S.J., Henderson, J.M., Karion, A., Lindaas, J., Melton, J.R., Miller, J.B., Sweeney, C., Wofsy, S.C., Michalak, A.M., 2016. A multiyear estimate of methane fluxes in Alaska from CARVE atmospheric observations. Glob. Biogeochem. Cycles 30, 1441–1453.
Minasny, B., Malone, B.P., McBratney, A.B., Angers, D.A., Arrouays, D., Chambers, A., Chaplot, V., Chen, Z.S., Cheng, K., Das, B.S., Field, D.J., Gimona, A., Hedley, C.B., Hong, S.Y., Mandal, B., Marchant, B.P., Martin, M., McConkey, B.G., Mulder, V.L., O'Rourke, S., Richer-de-Forges, A.C., Odeh, I., Padarian, J., Paustian, K., Pan, G., Poggio, L., Savin, I., Stolbovoy, V., Stockmann, U., Sulaeman, Y., Tsui, C.C., Vågen, T.G., van Wesemael, B., Winowiecki, L., 2017. Soil carbon 4 per mille. Geoderma 292, 59–86.
National Aeronautics and Space Administration, 2017. Global Daily Downscaled Climate Projections. (from). ftp://ftp.nccs.nasa.gov/BCSD/rcp45/day/atmos/, Accessed date: 20 June 2017.
Nemani, R.R., Keeling, C.D., Hashimoto, H., Jolly, W.M., Piper, S.C., Tucker, C.J., Myneni, R.B., Running, S.W., 2003. Climate-driven increases in global terrestrial net primary production from 1982 to 1999. Science 300, 1560–1563.
O'Rourke, S.M., Angers, D.A., Holden, N.M., McBratney, A.B., 2015. Soil organic carbon across scales. Glob. Chang. Biol. 21, 3561–3574.
Ouyang, W., Geng, X., Huang, W., Hao, F., Zhao, J., 2016. Soil respiration characteristics in different land uses and response of soil organic carbon to biochar addition in high-latitude agricultural area. Environ. Sci. Pollut. Res. 23, 2279–2287.
Padarian, J., Minasny, B., McBratney, A.B., 2015. Using Google's cloud-based platform for digital soil mapping. Comput. Geosci. 83, 80–88.
Pan, G., Xu, X., Smith, P., Pan, W., Lal, R., 2010. An increase in topsoil SOC stock of China's croplands between 1985 and 2006 revealed by soil monitoring. Agric. Ecosyst. Environ. 136 (1), 133–138.
Percival, D.P., 1995. On estimation of the wavelet variance. Biometrika 82, 619–631.
Post, W.M., Emanuel, W.R., Zinke, P.J., Stangenberger, A.G., 1982. Soil carbon pools and world life zones. Nature 298, 156–159.
Selmants, P.C., Litton, C.M., Giardina, C.P., Asner, G.P., 2014. Ecosystem carbon storage does not vary with mean annual temperature in Hawaiian tropical montane wet forests. Glob. Chang. Biol. 20, 2927–2937.
Shangguan, W., Dai, Y., Duan, Q., Liu, B., Yuan, H., 2014. A global soil data set for earth system modeling. J. Adv. Model Earth Syst. 6, 249–263.
Soleimani, A., Hosseini, S.M., Massah, B.A., Jafari, M., Francaviglia, R., 2017. Simulating soil organic carbon stock as affected by land cover change and climate change, Hyrcanian forests (northern Iran). Sci. Total Environ. 599–600, 1646–1657.
Stockmann, U., Adams, M.A., Crawford, J.W., Field, D.J., Henakaarchchi, N., Jenkins, M., Minasny, B., McBratney, A.B., de Courcelles, V.D.R., Singh, K., Wheeler, I., Abbott, L., Angers, D.A., Baldock, J., Bird, M., Brookes, P.C., Chenu, C., Jastrow, J.D., Lal, R., Lehmann, J., O'Donnellk, A.G., Parton, W.J., Whitehead, D., Zimmermann, M., 2013. The knowns, known unknowns and unknowns of sequestration of soil organic carbon. Agric. Ecosyst. Environ. 164, 80–99.
Stockmann, U., Padariana, J., McBratney, A.B., Minasny, B., de Brogniez, D., Montanarella, L., Hong, S.Y., Rawlins, B.G., Field, D.J., 2015. Global soil organic carbon assessment. Glob. Food Sec. 6, 9–16.
Wang, Y., Yu, Z., Li, Y., Wang, G., Liu, J., Liu, J., Liu, X., Jin, J., 2017. Microbial association with the dynamics of particulate organic carbon in response to the amendment of elevated CO2-derived wheat residue into a Mollisol. Sci. Total Environ. 607–608, 972–981.
WorldGrids, 2017. Global Environmental Layers. (from). http://worldgrids.org, Accessed date: 20 June 2017.
Yu, S., Chen, Y., Zhao, J., Fu, S., Li, Z., Xia, H., Zhou, L., 2017. Temperature sensitivity of total soil respiration and its heterotrophic and autotrophic components in six vegetation types of subtropical China. Sci. Total Environ. 607–608, 160–167.
Zhang, H., Wang, E., Zhou, D., Luo, Z., Zhang, Z., 2016. Rising soil temperature in China and its potential ecological impact. Sci Rep 6.
Zhou, Y., Biswas, A., Ma, Z., Lu, Y., Chen, Q., Shi, Z., 2016. Revealing the scale-specific controls of soil organic matter at large scale in Northeast and North China Plain. Geoderma 271, 71–79.